Cave Rings

Emma Boland[12]

October 13, 2010

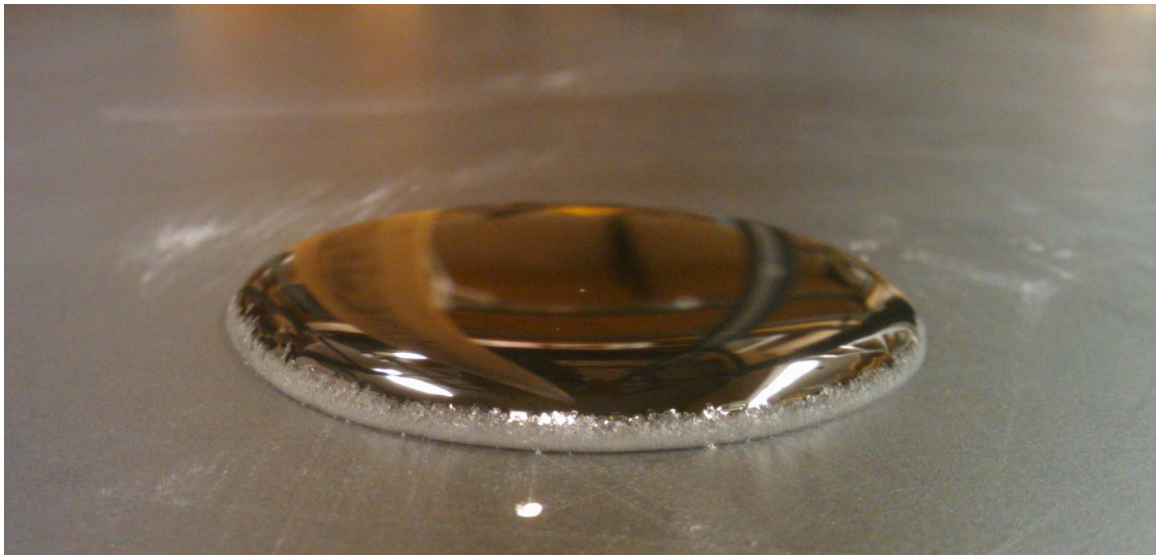

with Neil Balmforth[3] and Colm-Cille Caulfield[1]

1. The University of Cambridge, Cambridge, United Kingdom. 2. The British Antarctic Survey, Cambridge, United Kingdom. 3. The University of British Columbia, Vancouver, Canada.

1 Introduction

Cave Rings are cave formations, or speleothems, consisting of thin circles on cave floors, normally found surrounding a water splash point, beneath stalactites. The rings range in diameter from a few centimetres to roughly two metres, and the width and height of the deposit ranges from a few millimetres to a few centimetres. Examples from caves in Italy can be seen in figure 1. Elliptical formations have also been observed in locations with tilted cave floors. The rings tend to occur in locations where the floor is without strong flows, and with a layer of dust or mud, although it is not clear whether this merely aids their discovery, or is related to their formation.

Report Documentation Page

Form Approved
OMB No. 0704-0188

1. REPORT DATE	2. REPORT TYPE	3. DATES COVERED
13 OCT 2010		**00-00-2010 to 00-00-2010**

4. TITLE AND SUBTITLE	5a. CONTRACT NUMBER
Cave Rings	5b. GRANT NUMBER
	5c. PROGRAM ELEMENT NUMBER
6. AUTHOR(S)	5d. PROJECT NUMBER
	5e. TASK NUMBER
	5f. WORK UNIT NUMBER
7. PERFORMING ORGANIZATION NAME(S) AND ADDRESS(ES) **Woods Hole Oceanographic Institution,Woods Hole,MA,02543**	8. PERFORMING ORGANIZATION REPORT NUMBER
9. SPONSORING/MONITORING AGENCY NAME(S) AND ADDRESS(ES)	10. SPONSOR/MONITOR'S ACRONYM(S)
	11. SPONSOR/MONITOR'S REPORT NUMBER(S)

12. DISTRIBUTION/AVAILABILITY STATEMENT
Approved for public release; distribution unlimited

13. SUPPLEMENTARY NOTES
See also ADA544302

14. ABSTRACT

Cave Rings are cave formations, or speleothems, consisting of thin circles on cave floors,normally found surrounding a water splash point, beneath stalactites. The rings range in diameter from a few centimetres to roughly two metres, and the width and height of the deposit ranges from a few millimetres to a few centimetres. Examples from caves in Italy can be seen in figure 1. Elliptical formations have also been observed in locations with tilted cave floors. The rings tend to occur in locations where the floor is without strong flows, and with a layer of dust or mud, although it is not clear whether this merely aids their discovery, or is related to their formation.

15. SUBJECT TERMS

16. SECURITY CLASSIFICATION OF:			17. LIMITATION OF ABSTRACT	18. NUMBER OF PAGES	19a. NAME OF RESPONSIBLE PERSON
a. REPORT	b. ABSTRACT	c. THIS PAGE			
unclassified	**unclassified**	**unclassified**	**Same as Report (SAR)**	**29**	

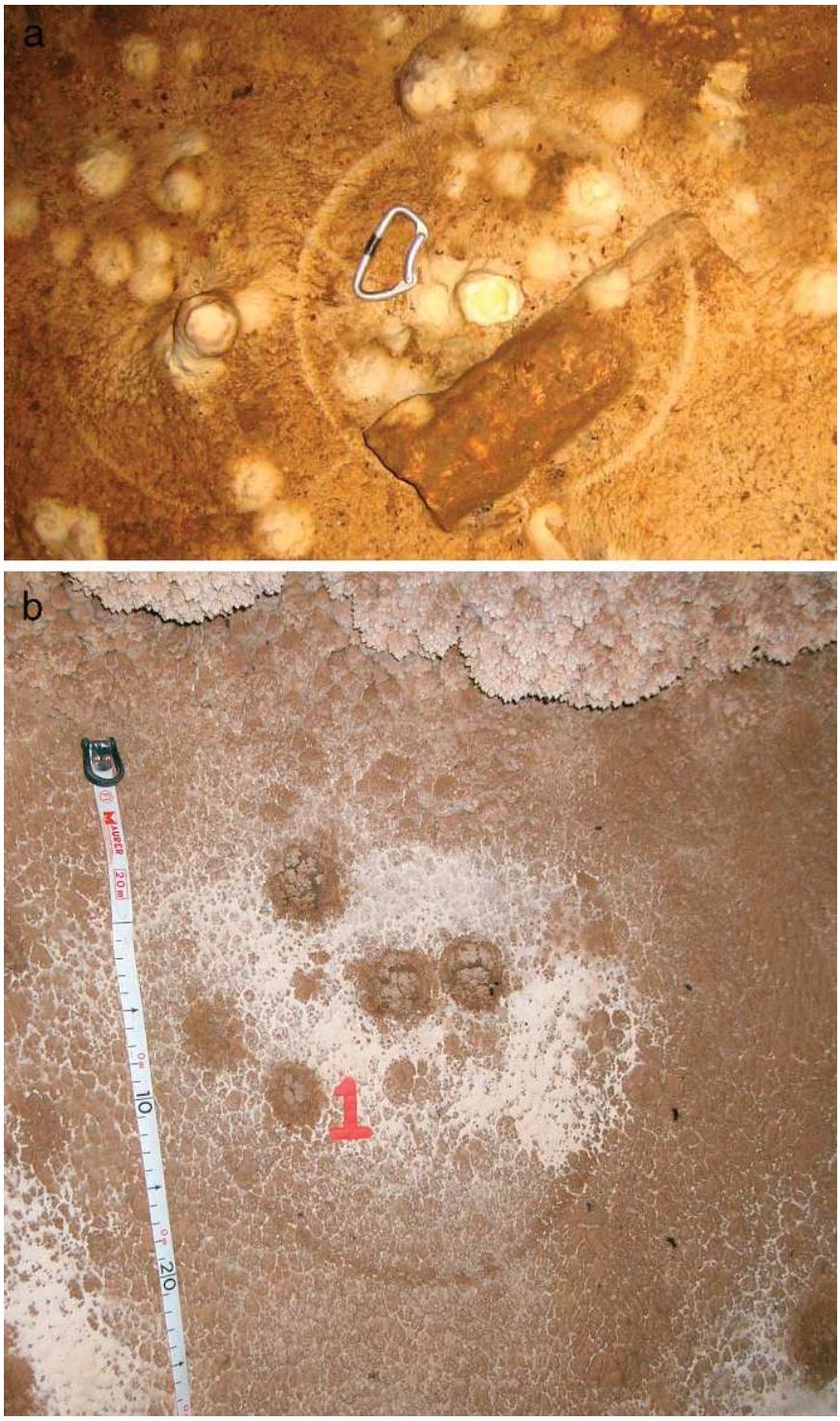

Figure 1: Rings photographed in a) Grotta Imbroglita and b) Grotta del Secchio in Italy, from [9]

There are currently two theories within the caving community as to the method of ring formation. The first, designated the 'splash ring' mechanism, is thought to be the method responsible for producing the larger rings, and postulates that the rings are formed due to the accumulation of deposits from secondary drops being ejected from the primary drop site [5, 9]. This requires that the majority of the secondary drops fall to the same radius. This is explained in [5] as being due to the majority of the drops ejecting at 45° and then travelling a distance determined by the kinetic energy of the primary drop, dependent on the height of the source above the floor.

The second theory, designated the 'fall down ring' mechanism, thought to be responsible for the smaller sized rings, was first proposed in [8] and theorises that the rings are formed due to the accumulation of secondary drops produced from the spontaneous breakup of the primary drop during its fall. In [9], Nozzoli et al. claim to prove through analysis of collected data from various rings that this is in fact the method responsible for the formation of all cave rings. They suggest that all of the primary drops break up at 142.7±7.2 cm from the stalactite tip and then fall in a *negative* arc to the floor, due to 'other forces' than gravity acting on the small secondary drops.

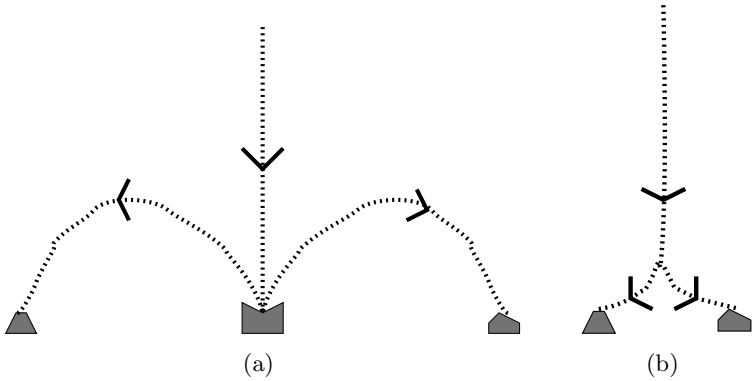

Figure 2: Depiction of a) the 'splash ring' hypothesis and b) the 'fall down ring' hypothesis.

The aim of this project is to show, through analysis and experiments, that both the 'splash ring' and 'fall down ring' hypotheses are clearly false. We also test a new hypothesis, that cave rings are formed in the same manner as coffee rings[3], that is, due to the enhanced deposition at the edges of sessile drops.

2 Experimental Setup

In the following section, the experimental setup used throughout is described. A depiction of the equipment used can be seen in figure 3. Throughout salt water was used as an analogue to the water found in caves. The accuracy of this replacement is discussed in section 6

A black aluminium sheet, 122 cm by 66 cm, was used as a surface which could be easily heated and also provide contrast to the white salt crystals. This was raised a few cm off the floor, and levelled using a spirit level, although the sheet was not flat to high precision. Underneath were 6 fluorescent light tubes, centred in the width of the sheet and evenly

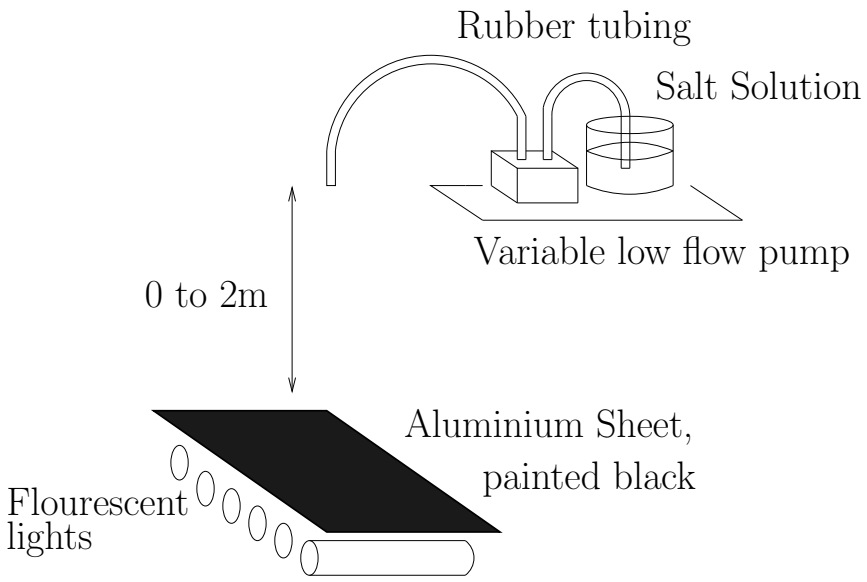

Figure 3: Depiction of the experimental setup used throughout.

distributed along the length of the sheet. These were on for the duration of all experiments, and left on for several hours before any experiment began, to provide even heating to encourage evaporation, reducing the time scales of the experiments. The sheet reached temperatures of 25-27°C, and was fairly consistent in time, though not evenly distributed across the sheet.

Above this sheet was a system of rubber tubing connecting a variable low flow pump with a source of salt solution, which was varied in concentration for different experiments. The solution was pumped at a constant, controllable rate. The calibration of the pump was carried out by collecting the liquid pumped over a period of time for a specific setting, then using a combination of accurate weight and density measurements, the volume pumped per hour was found. It was noted that the rate was very consistent between different measurements. The end of the tube was suspended over the table using system of pulleys and string, and thus the height above the table could be adjusted between 0 and 2m.

A Nikon D200 model digital SLR camera was set up on a tripod next to the table to record images from experiments. This was set on a timer to take images at 15 minute intervals throughout all experiments. The images were then processed using the Image Processing Toolbox in the Matlab 2010a software program.

3 Splash Ring Conjecture

3.1 Literature

The 'splash ring' conjecture is described in [5]. It is claimed that 45° is the most probable angle for secondary drops to be ejected at, and that the subsequent radius of the ring is determined by the amount of kinetic energy imparted to the primary drop on its fall from the stalactite tip. This has several logical flaws, the most obvious being the assumption that the

secondary drops will almost always gain the same amount of kinetic energy from the splash, and therefore land at the same radius from the splash site every time. The work of [1] shows that, in the case of drops hitting a very shallow liquid layer, as is likely under stalactites, there is a range of emission angles and a wide range of emission velocities, resulting in a range of splash radii. The literature surrounding the investigation of the transport of soil and plant pathogens via raindrops uses a 'Fundamental Splash Distribution Function' which assumes that the mass splashed falls exponentially with radius, see e.g. [10], and is confirmed experimentally.

3.2 Experiment

In order to experimentally disprove the splash ring conjecture, the setup described in section 2 was used, with the source raised 2m above the sheet, and a 15% salt solution was dripped at a rate of 17.7 ± 0.5 ml per hour. The resulting pattern of salt crystals left on the sheet after 19 hrs 15 min can be seen in figure 4(a), where the image has been manipulated to highlight the location of the salt crystals as follows, using the *Image Processing Toolbox* in Matlab 2010a:

1. Background gradients due to lighting removed.
2. Image converted to greyscale.
3. Exposure adjusted to rescale pixels with an intensity index of greater than 0.5 to an index of 1.
4. Image converted to black and white.
5. Image taken before experiment started removed to eliminate background items.

The pattern seen in the bottom right of the photo is due to reflections of drops from a piece of equipment located next to the sheet, and so all numerical calculations from this image use the upper half of the splash pattern only. This experiment was not designed to imitate cave conditions, but to demonstrate clearly the distribution of secondary drops produced by a single drop.

The distribution of salt coverage, a proxy for drop mass, versus radius can be seen in figure 4(b), as calculated from the image in figure 4(a). The salt coverage ratio is calculated from the ratio of white to black pixels within a given radius range. The radius is calculated by finding the length of a pixel in an image using the known dimensions of the sheet. At small radii, there is no salt due to the constant recycling of the water beneath the source preventing crystallisation from occurring. From roughly 4-10cm, the surface is completely covered in salt crystals, and so the Salt Coverage Ratio is saturated at a value of 1. The method of using photographs from above the table means that the thickness of the salt at this point cannot be determined. The fact that some radii appear to have coverage ratios greater than one is due to the limitations of the technique employed: because the camera could not be placed directly over the sheet due to the presence of the source equipment, the pictures are taken at a slight angle, and so each pixel is not the same length, as assumed in calculations. There are also inherent errors in taking radial calculations from gridded data. However, this experiment was not intended to provide accurate numerical data, merely

to provide a qualitative demonstration of the inaccuracy of the 'splash ring' conjecture. The clear exponential tail to the distribution at radii greater than 10cm shows qualitative agreement with the literature as discussed in section 3.1.

To determine whether the presence of a central stalagmite could have an effect on the location of splashes, the same experiment was repeated, but with an upturned Pyrex beaker placed under the centre of the source, see figure 5(a). A 20% salt solution was dripped at a rate of 10.1 ± 0.6 ml per hour, and the resulting pattern left after 21.5 hours can be seen in figure 5(b). Clearly there is no ring formed, and the pattern formed is similar to that formed with the stalagmite absent, although, as the flow rate was lower, the pattern is not as large.

4 Fall Down Ring Conjecture

4.1 Literature

The 'fall down' ring conjecture was first proposed in [8] as an explanation for the smaller sized cave rings observed. In [9], Nozzoli et al. claim to prove that all cave rings are produced by this method. They collected data from 67 rings in 5 caves in Central Italy, as well as creating some artificial rings by placing wooden tablets covered in soot underneath several stalactites, over rings. The data they collected can be seen in figure 6, where an apparent correlation between the height of the source stalactite and the ring radius can be seen. They fit this data to a quadratic function, and then conclude that all the rings are produced by drops that break up at 142.7 ± 7.2 cm below the source stalactite, then execute a *negative* arc to the ring radius. To conclude, because a curve can be fitted to the data, that the theory must therefore be correct, is optimistic at best. There could be many ways to explain a relationship between the two quantities measured, and there is no explanation as to the mechanism behind the proposed breakup, or the physically unlikely negative curvature, which is put down to 'unknown' forces. There is also an apparent contradiction in their explanation - if the drops always break up, then what forms the central stalagmite visible at the centre of all the rings? The artificial rings, which they claim were formed on the wooden tablets over a period of roughly 20 days, would perhaps be more convincing if the paper contained any pictures of these rings or a fuller explanation of what was found. The only thing to be concluded from this work is that any successful production theory must explain this apparent correlation between source height and ring radius.

A review of the literature involving drop breakup revealed the extensive study of Villermaux and Bossa[11] into the dynamics of single drop deformation and breakup, with the aim of explaining the distribution of raindrop sizes found at ground level. The condition for drop break up is $W_e > 6$, where W_e is the Weber number of the drop. For such a drop, first it pancakes and then the radius increases exponentially with time until breakup. If $W_e < 6$, the drop pancakes but then oscillates around a mean radius. For a drop falling in static air, the Weber number is defined as the ratio between the gravitational force on the droplet and the surface tension on the drop:

$$W_e = \frac{\rho g d^2}{\sigma}, \tag{1}$$

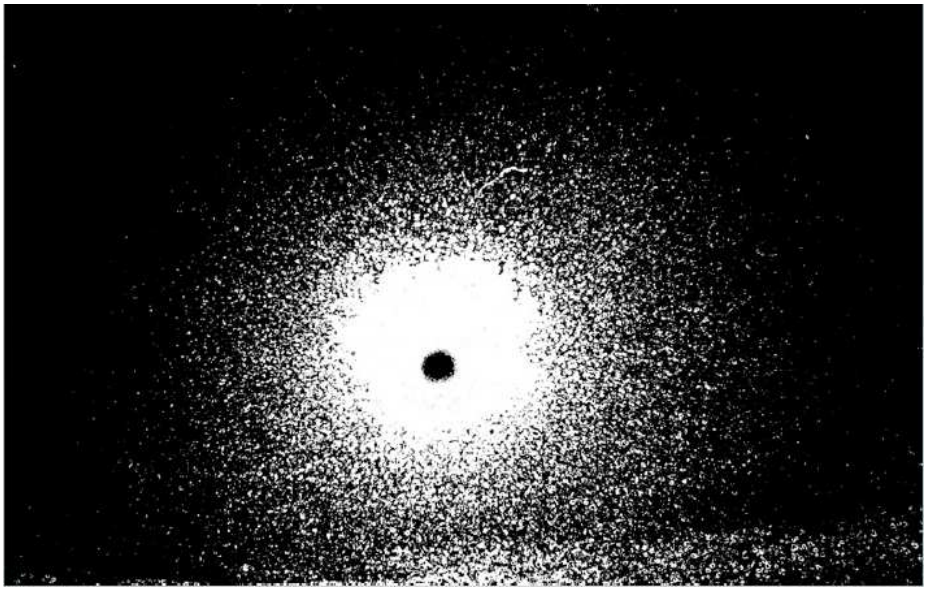

(a)

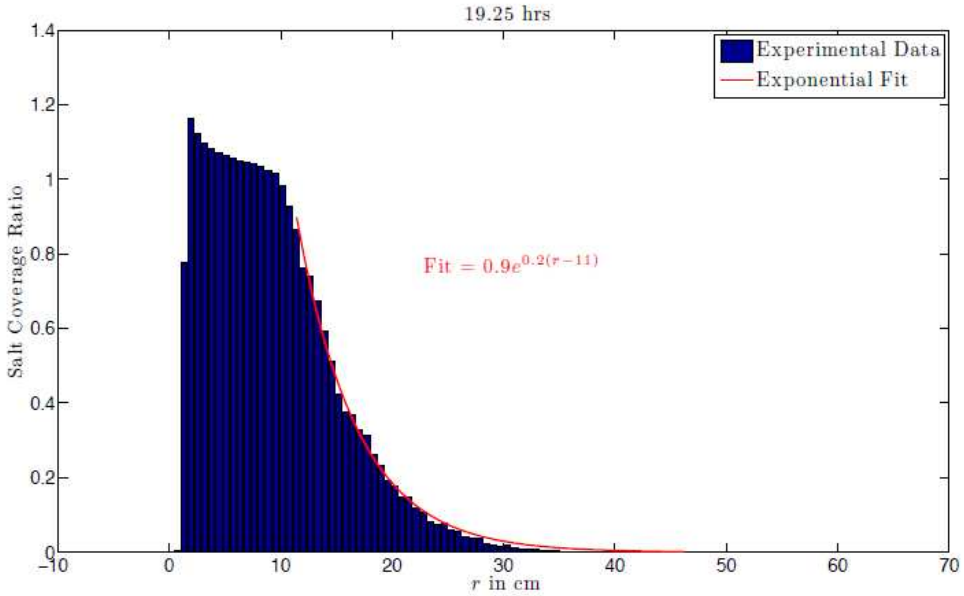

(b)

Figure 4: Experiment described in section 3.2 after 19.25 hours. (a) shows a photo of the sheet, with the exposure manipulated to highlight the salt crystals. (b) shows the salt coverage ratio versus radius, calculated from the image in (a), showing a clear exponential tail to the distribution.

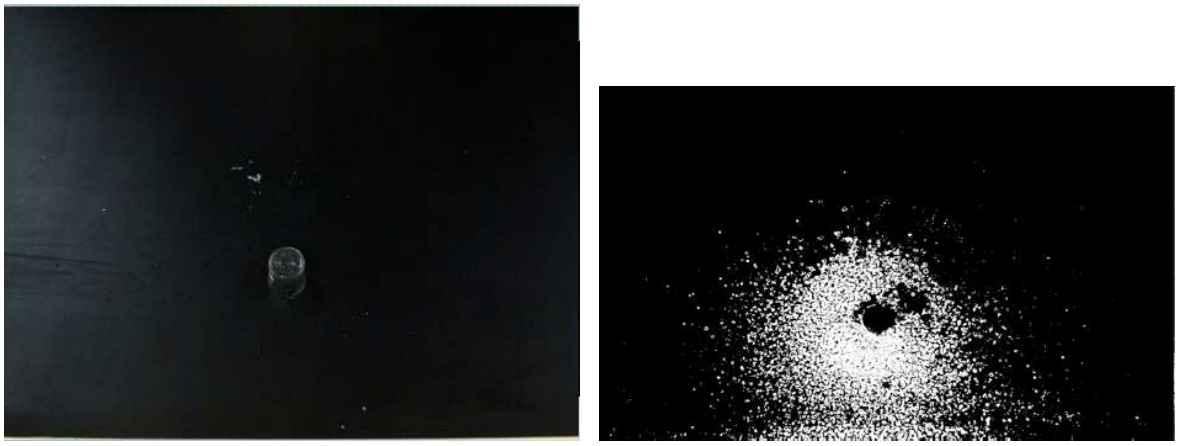

(a) (b)

Figure 5: Experiment as described with Pyrex beaker to represent a stalagmite. (a) shows the beaker in place on the aluminium sheet. (b) shows a manipulated photo to highlight the salt crystals present after 21.5 hours.

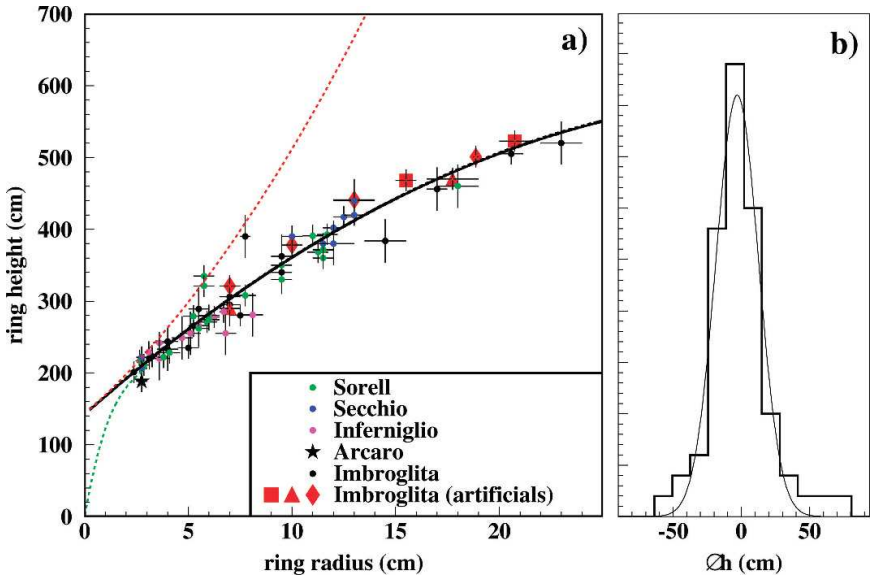

Figure 6: Figures from [9], showing a) the measured height of the source above the rings vs the radius of the ring, for the in situ rings and the artificial rings (large red symbols). The solid black line shows the best fit 2nd degree polynomial. b) shows the distribution of the difference between the best fit height and the actual height.

where ρ is the density of the water, g is gravitational acceleration, d is the diameter of the drop and σ is the surface tension between the water and the air. For a pendant drop, such as one forming on a stalactite, at detachment the gravitational force on the drop just exceeds the surface tension, i.e.

$$\frac{1}{6}\pi g\rho d^3 \approx \pi D\sigma, \tag{2}$$

where D is the diameter of the source. Combining (1) and (2) gives $W_e \approx 6D/d$. and thus the condition for the drop to breakup becomes $D > d$, i.e. the drop must detach whilst its diameter is less than that of the source. This is physically unlikely for a detaching pendant drop, see for example [4] and figure 7, and implies the drop would initially have a diameter of over 7cm.

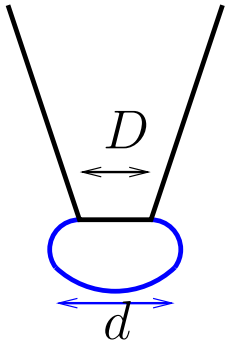

Figure 7: Depiction of a pendant drop from a stalactite. D is the diameter of the source of liquid and d is the diameter of the drop itself.

4.2 Experiment

To disprove the 'fall down' conjecture experimentally, the setup described in section 2 was used, with the source raised 2m above the sheet, and a 20% salt solution was pumped at a rate of 17.7 ± 0.5 ml per hour. A plastic beaker was placed on the sheet directly below the source, in order to catch the primary drop. The experiment was run for 22 hours, after which the beaker contained the majority of the water; a small amount had bounced out as the beaker began to fill, see figure 8. No drops were observed breaking up throughout any of the experiments. It must be noted that 2m is at the lowest end of the observed rings, see figure 6, and that a higher fall height would be more rigorous in disproving the 'fall down' conjecture, however 2m was the limit of the equipment available.

5 Coffee Ring Theory

A 'coffee ring' is the deposit formed when a sessile drop of a solution containing dissolved particles, such as coffee or salt, dries. This was investigated by Deegan et. al in [3], and shown to be the result of a combination of contact line pinning and non-uniform evaporation flux. If the contact line of a drop is pinned, by a slightly rough surface for example, then,

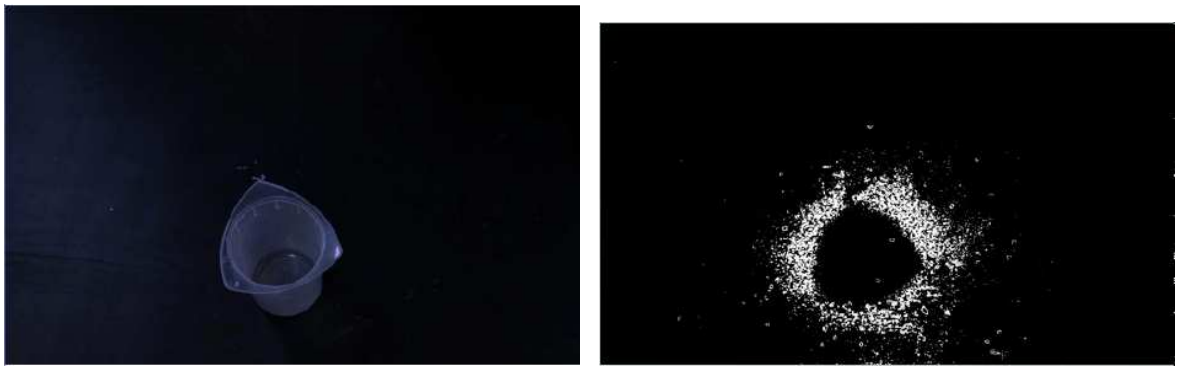

(a) (b)

Figure 8: Experiment as described with plastic beaker to catch primary drops. (a) shows the beaker in place on the aluminium sheet. (b) shows a manipulated photo to highlight the salt crystals present after 22 hours.

when volume is lost, the majority is taken from the centre of the drop, see figure 9. The rate limiting step in evaporation from a drop is the diffusion of water vapour away from the saturated region around the drop. Due to the geometry of the drop, assumed to be close to a spherical cap, the evaporation is enhanced at the contact line, where it is easier for a water vapour particle to escape, see figure 10(a).

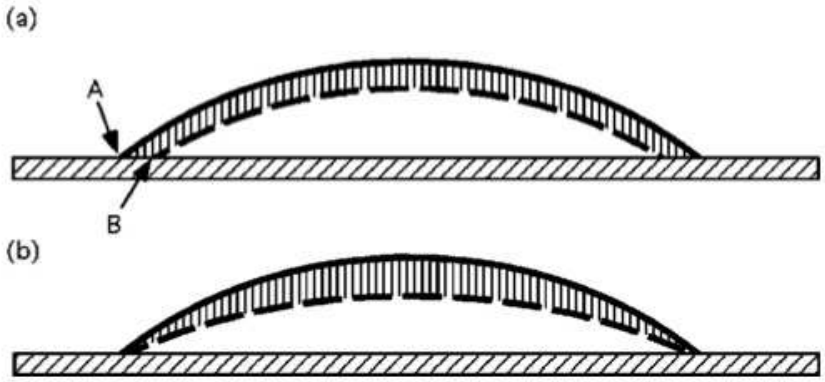

Figure 9: Depiction of volume lost from (a) a drop where the contact line is free to move and (b) a drop where the contact line is pinned. [3]

Because of the mis-match in the location of maximum mass loss and maximum evaporation flux, see figure 10(b), there is a constant flux of fluid towards the edge of the drop to replace the evaporated water. As the majority of the evaporation occurs at the edge of the drop, the majority of the dissolved particles are deposited at the edge of the drop, resulting in the visible ring left behind.

While this is a well formed theory for drops of the size of a few cm or less, it was proposed that this could also be the mechanism behind the formation of cave rings. If the

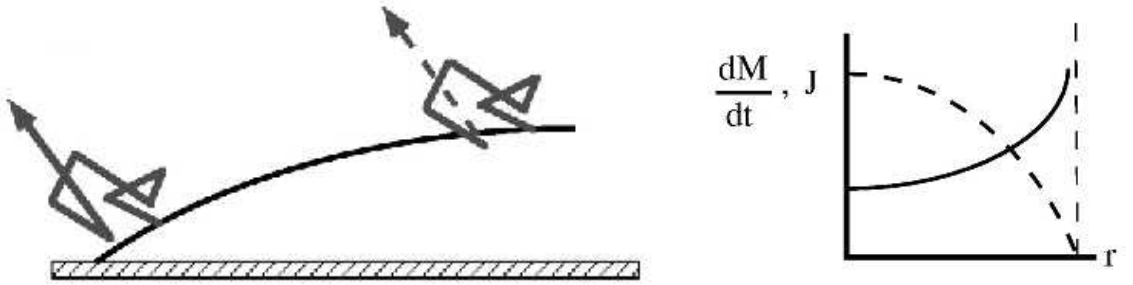

(a) (b)

Figure 10: (a) Depiction of a water vapour particle performing a random walk at the edge of the drop. It is more likely to escape near the contact line. (b) Magnitude of mass loss, dM/dt, dashed line, and evaporation flux, J, line, versus radius of the drop. The evaporation flux is singular at the contact line. [3]

flow rate in the cave was high enough to produce a large puddle, perhaps perhaps during a rain storm, then the coffee ring mechanism could produce a ring of limestone deposit around the edge of the puddle, forming the cave ring left behind.

5.1 Large Coffee Ring model

5.1.1 Large Puddle

To test the 'coffee ring' hypothesis, we developed a model for large coffee rings. We begin by modelling a large puddle, fed by a source and losing water to evaporation, with a surface described by $h(r,t)$, using the 2-D quantities depicted in figure 11, under the following assumptions:

- slow, viscous flow,
- shallow puddle, $R >> H$,
- source within $r = a$,
- no slip at $z = 0$,
- no stress at $z = h$.

The momentum balance in the radial and vertical directions can then be written as follows:

$$\frac{1}{\rho}\frac{\partial p}{\partial r} = \nu\frac{\partial^2 u}{\partial z^2} + smaller, \tag{3}$$

$$\frac{1}{\rho}\frac{\partial p}{\partial z} = g + smaller, \tag{4}$$

where $p\,(r,z,t)$ is the pressure in the puddle, ρ is the density of the fluid (assumed constant), ν is the molecular diffusivity of the fluid, and g is gravitational acceleration. These

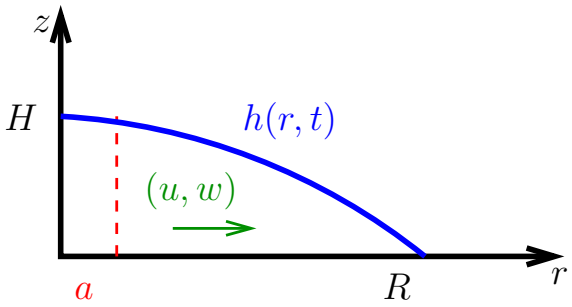

Figure 11: Depiction of the quantities described in the large puddle model. $h(r,t)$ is the surface of the puddle, (u,w) is the velocity field withing the puddle, H and R are the vertical and radial scales respectively, and a is the radius containing the source.

expressions, along with the boundary conditions previously mentioned, lead to the following definitions of the pressure, p and horizontal velocity, u:

$$p = \rho g(h - z), \qquad u = \frac{g}{\nu}\frac{\partial h}{\partial r} z(z - 2h). \tag{5}$$

Mass conservation leads to the following relation between the horizontal and vertical velocities, u and w respectively:

$$\nabla \cdot v = \frac{1}{r}\frac{\partial}{\partial r}(ru) + \frac{\partial w}{\partial z} = 0. \tag{6}$$

Integrating (6) in the vertical:

$$\int_0^z \frac{1}{r}\frac{\partial}{\partial r}(ru)\, dz + w(z) - w(0) = 0. \tag{7}$$

The dynamical boundary conditions for w are as follows:

$$w(z = h) = \frac{\partial h}{\partial t} + u \cdot \frac{\partial h}{\partial r}\bigg|_{z=h} + w_{evap}, \tag{8}$$

$$w(z = 0) = H(a - r) w_{source}, \tag{9}$$

where w_{evap} and w_{source} are the vertical velocities of fluid leaving via evaporation and entering from the source respectively, and $H(a - r)$ is a Heaviside function. We have assumed here that the source is placed at $z = 0$, but the results that follow are the same if the source is instead assumed to be at $z = h$. If we evaluate (7) at $z = h$:

$$\int_0^h \frac{1}{r}\frac{\partial}{\partial r}(ru)\, dz + u \cdot \frac{\partial h}{\partial r}\bigg|_{z=h} + \frac{\partial h}{\partial t} + w_{evap} - H(a - r) w_{source} = 0, \tag{10}$$

$$\frac{1}{r}\frac{\partial}{\partial r}\left(r \int_0^h u\, dz\right) + \frac{\partial h}{\partial t} + w_{evap} - H(a - r) w_{source} = 0. \tag{11}$$

The form of w_{evap} can be found from Hu and Larson[6], who expanded on Deegan et al.[3] to find an exact form for the evaporation flux over a sessile drop. It turns out that solving

for the flux is equivalent to the problem of deriving the electrostatic potential formed by the union of two spherical caps, as previously solved by Lebedev[7]. Taking the form for a spherical cap with contact line angle equal to zero, assuming that for a large puddle that this will be approximately correct, then

$$w_{evap} = \frac{\kappa}{\sqrt{R^2 - r^2}}, \quad \kappa = \frac{2D\rho_v(1-\theta)}{\pi\rho}, \tag{12}$$

where R is the radius of the puddle, D is the molecular diffusivity of water vapour in air, ρ_v is the saturated vapour density of water, ρ is the density of liquid water, and θ is the ambient relative humidity.

Combining (5), (11) and (12), the evolution of the puddle height can be written as follows:

$$\frac{\partial h}{\partial t} = H(a-r)\frac{q}{\pi a^2} - \frac{\kappa}{\sqrt{R^2 - r^2}} + \frac{2g}{3\nu}\frac{1}{r}\frac{\partial}{\partial r}\left(r\frac{\partial h}{\partial r}h^3\right), \tag{13}$$

where q is the source flux in m^3/s. Assuming a steady state, i.e. $\partial h/\partial t = 0$, then we can solve for the height profile of the puddle, h:

$$h(r) = 2^{1/4}\left[g(r) + H(r-a)\left[\frac{1}{2}\left(1 - \frac{r^2}{a^2}\right) + \log\left(\frac{r}{a}\right)\right]\right]^{1/4}, \tag{14}$$

$$g(r) = \log\left(\frac{r}{1-\sqrt{1-r^2}}\right) - \sqrt{1-r^2}, \tag{15}$$

where the parameters have been non-dimensionalised as follows: $h \to h/H$, $r \to r/R$, $a \to a/R$. The non-dimensional height and radial scales are defined as follows:

$$R = \frac{q}{2\pi\kappa}, \quad H = \left(\frac{3\nu q}{2\pi g}\right)^{1/4}. \tag{16}$$

The form of $h(r)$ can be seen in figure 12 for $a = 0.1$.

5.1.2 Solute Dynamics

We now include the concentration of a passive solute, such as salt or coffee, $c(r, z, t)$, and consider a section of the puddle from r_1 to r_2 and $z = 0$ to $z = h$, as depicted in figure 13. If we require conservation of c over the section, then this implies:

$$\frac{\partial}{\partial t}\int_{r_1}^{r_2}\int_0^{h(r,t)} c(r,z,t)\,dz\; r\,dr = -\left[r\int_0^{h(r,t)} J_r(r,z,t)\;dz\right]_{r_1}^{r_2} + \int_{r_1}^{r_2} rc(r,0,t)w(r,0,t)\,dr, \tag{17}$$

where $J_r(r, z, t)$ is the radial flux of solute, and the solute arrives through the bottom with flux $J_z(r, z = 0, t) \equiv w(r, z = 0, t)c(r, z = 0, t) = w_{source}c_{source}$, but the solute cannot leave the puddle through evaporation, and so the flux of concentration at $z = h$ is zero. If we rewrite (17) as a single integral over (r_1, r_2), set the integrand to zero since the limits are arbitrary, and use the definition of $\mathbf{J} = c\mathbf{u} - \chi\nabla c$, we get

$$\frac{\partial}{\partial t}\int_0^{h(r,t)} c(r,z,t)\,dz = -\frac{1}{r}\frac{\partial}{\partial r}\left[r\int_0^{h(r,t)}\left(c(r,z,t)u(r,z,t) - \chi r\frac{\partial c}{\partial r}\right)\;dz\right] + c_{source}w_{source}, \tag{18}$$

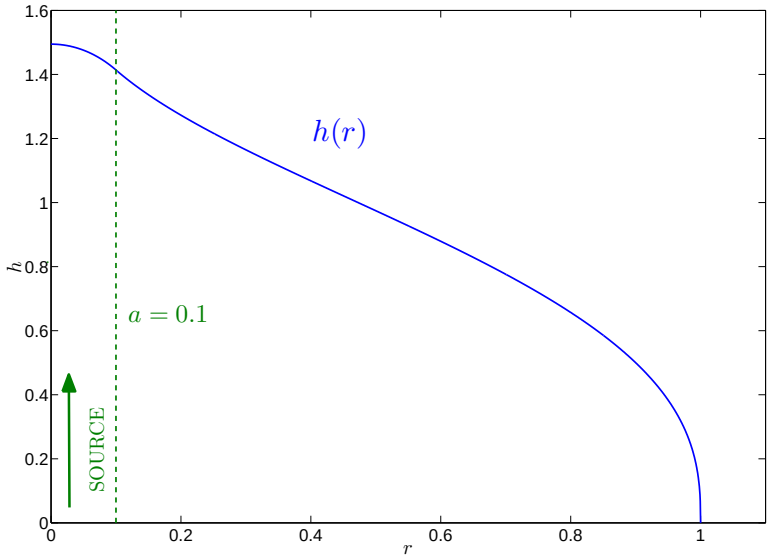

Figure 12: The steady state solution $h(r)$, the height of the puddle, see (14), for $a = 0.1$.

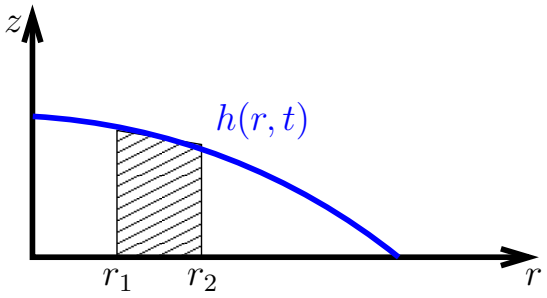

Figure 13: Depiction of section of puddle considered in section 5.1.2.

where χ is the molecular diffusivity of the passive solute.

If we now consider the dimensions of each of the terms in the advection-diffusion equation, then we find the following balance:

$$\begin{array}{ccccc} \frac{\partial c}{\partial t} + \frac{1}{r}\frac{\partial}{\partial r}(ruc) + \frac{\partial}{\partial z}(wc) & = & \chi\frac{1}{r}\frac{\partial}{\partial r}(r\frac{\partial c}{\partial r}) & + & \chi\frac{\partial^2 c}{\partial z^2}, \\ \frac{uc}{R} & = & \frac{\chi c}{R^2} & + & \frac{\chi c}{H^2}, \end{array} \tag{19}$$

where the bottom row indicates the dimension. The second term on the RHS dominates on that side due to the shallow puddle assumption made previously, $R >> H$. Thus, the ratio between the left and right sides becomes $uH^2/R\chi = H/R.\mathrm{Pe}$, where Pe is the Peclet number of the fluid. The Peclet number is likely to not be large in a dripping cave fluid, and so the vertical diffusion term clearly dominates. Thus, we can assume that vertical diffusion acts fast enough to homogeonize the solute over the depth of the fluid, i.e. $c(r,z,t) \approx \bar{c}(r,t)$, and we find the following expression for the evolution of the concentration flux from (18):

$$\frac{\partial}{\partial t}(h\bar{c}) = -\frac{1}{r}\frac{\partial}{\partial r}(r\bar{c}\bar{u}) + H(a-r)w_s c_s + \chi\frac{1}{r}\frac{\partial}{\partial r}\left(r\frac{\partial \bar{c}}{\partial r}h\right), \tag{20}$$

where the subscript s denotes source properties, and $\bar{u}$ is the vertically integrated horizontal velocity u. From now on we will drop the bar over c.

If we first consider the simpler case of the steady state, $\partial h/\partial t$, then we can rewrite (20) as follows:

$$h\frac{\partial c}{\partial t} = H(a-r)\frac{c_s}{a^2} + \frac{1}{r}\frac{\partial}{\partial r}\left[r\left(c\frac{\partial h}{\partial r}h^3 + K\frac{\partial c}{\partial r}h\right)\right], \tag{21}$$

where $K = \pi\chi H/q$, $\tau = Hq/4\pi\kappa^2$, and the parameters have been non-dimensionalised as follows: $c \to c/c_0$, $c_s \to c_s/c_0$, $t \to t/\tau$, and h and r as previously, where c_0 is the initial concentration of the solute within the puddle, and h is described in (14).

Solving this numerically as an initial value problem using the *pdepe* routine in Matlab 2010a, the results up to $t = 0.9$ can be seen in figure 14, where $a = 0.1$, $c_s = 1$ and $K = 0.01$. It can be seen that, as expected, the solute is swept to the edge of the puddle over time, where it collects.

(21) can also be solved analytically in certain regimes. It can be seen from figure 14 that, away from the edge of the puddle ($r = 1$), the solution for $c(r)$ approaches a single solution over time. To solve for this solution we thus set $\frac{\partial c}{\partial t} = 0$. We also assume that, as the gradients in c are not large away from $r = 1$, that diffusion can be neglected (K being small). We are thus left with the following expression to solve:

$$\frac{1}{r}\frac{\partial}{\partial r}\left(rc\frac{\partial h}{\partial r}h^3\right) \approx -H(a-r)\frac{c_s}{a^2}. \tag{22}$$

Using (14), we can evaluate:

$$r\frac{\partial h}{\partial r}h^3 = -\frac{1}{2}\left[\sqrt{1-r^2} + H(a-r)\left(\frac{r^2}{a^2} - 1\right)\right], \tag{23}$$

and so can solve (22), using the boundary condition of zero flux at $r = 0$, and matching fluxes at $r = a$, to find:

$$c \approx \begin{cases} c_s, & r < a, K \approx 0, \\ c_s/\sqrt{1-r^2}, & r > a, K \approx 0. \end{cases} \tag{24}$$

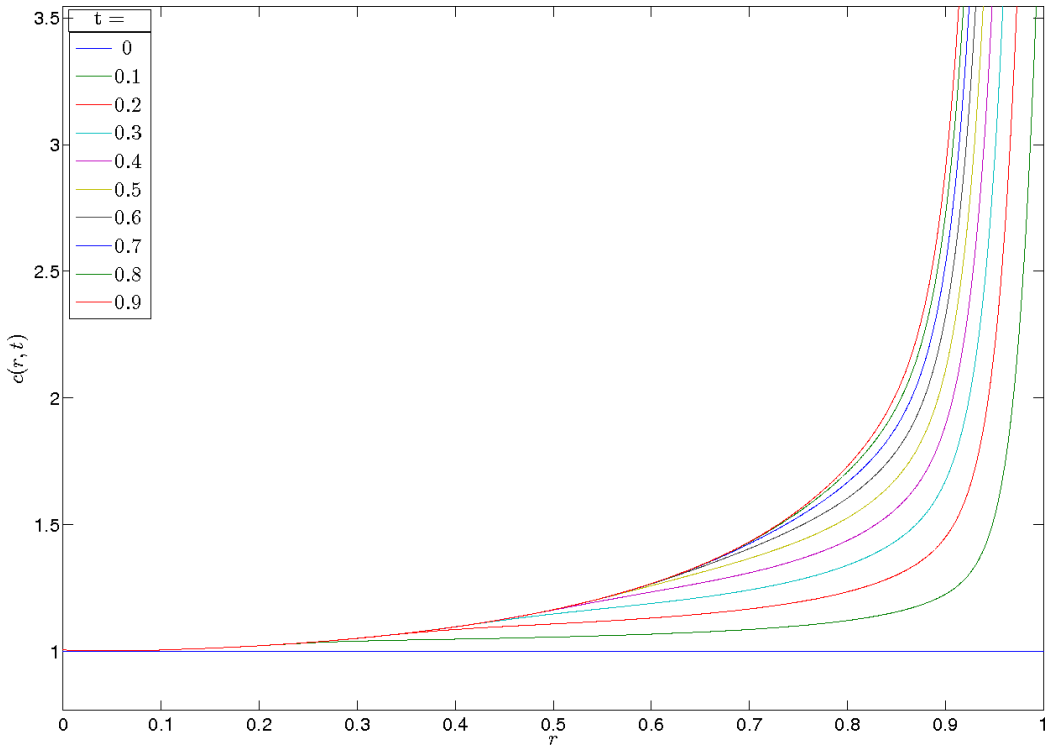

Figure 14: Solutions of (21) for $t = 0$ to 0.9, with $a = 0.1$, $c_s = 1$ and $K = 0.01$.

Thus, the solution matches the source concentration within the source area, and outside follows the evaporation profile (12). Comparing with the numerical solution, see figure 15, it can be seen that the analytical solution is best for low r, and becomes worse as the gradient of c increases, and diffusion becomes more important. At values of r close to to 1 and large times, the numerical solution for c becomes linear, see figure 16.

Thus, we can assume that $c(r,t)$ takes the form $A(r)t + B(r)$ near $r = 1$. Introducing this into (21), we get two coupled equations describing A and B:

$$0 = \frac{1}{r}\frac{\partial}{\partial r}\left[r\left(A\frac{\partial h}{\partial r}h^3 + K\frac{\partial A}{\partial r}h\right)\right], \tag{25}$$

$$hA = \frac{1}{r}\frac{\partial}{\partial r}\left[r\left(B\frac{\partial h}{\partial r}h^3 + K\frac{\partial B}{\partial r}h\right)\right]. \tag{26}$$

We initially concentrate on (25), and redefine r in terms of the parameter ζ, which is small near the puddle edge: $r = 1 - K^\alpha\zeta$. We can approximate h near $r = 1$, and find:

$$h \approx \left(\frac{2}{3}\right)^{1/4} 2^{3/8}(1-r)^{3/8} = \left(\frac{2}{3}\right)^{1/4} 2^{3/8}K^{3\alpha/8}\zeta^{3/8}, \tag{27}$$

and from (23) we can rewrite:

$$r\frac{\partial h}{\partial r}h^3 \approx -\frac{\sqrt{2}}{2}\sqrt{1-r} = -\frac{1}{\sqrt{2}}K^{\alpha/2}\zeta^{1/2}, \tag{28}$$

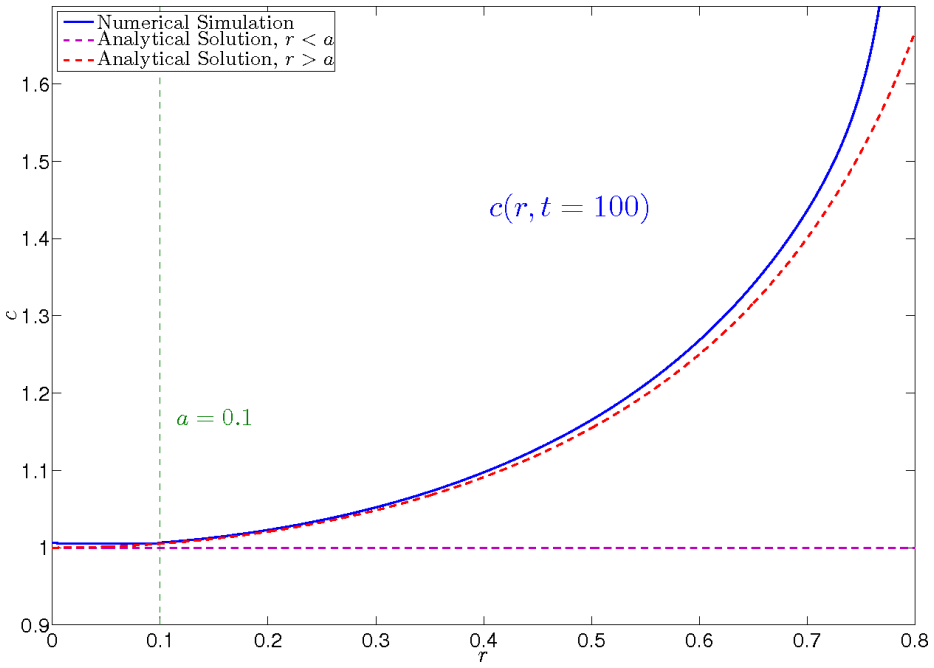

Figure 15: Comparison of the analytical and numerical solutions for $c(r)$ at large times away from $r = 1$.

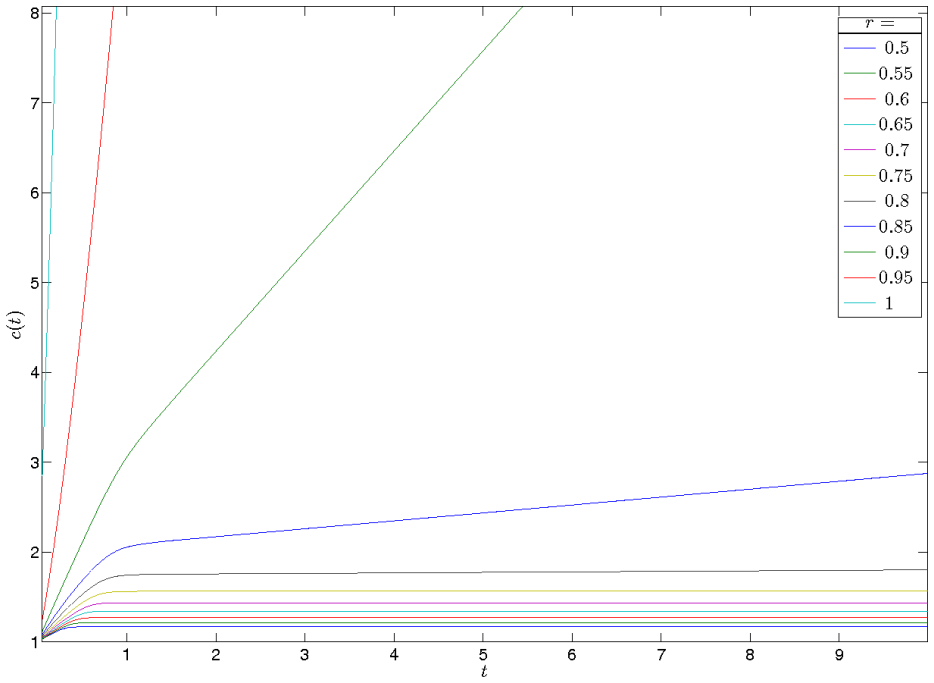

Figure 16: Numerical solutions for $c(t)$ at various radii. Close to $r = 1$, the concentration becomes linear with time.

and so (25) can be rewritten:

$$r\left(A\frac{\partial h}{\partial r}h^3 + K\frac{\partial A}{\partial r}h\right) \approx -A\frac{1}{\sqrt{2}}K^{\alpha/2}\zeta^{1/2} + K^{1-\alpha}\frac{\partial A}{\partial \zeta}\left(\frac{2}{3}\right)^{1/4} 2^{3/8}K^{3\alpha/8}\zeta^{3/8} = 0, \quad (29)$$

where we have integrated both sides. The integration constant is zero, as the expression is equal to zero at $r = 0$. Rearranging:

$$\left(\frac{2}{3}\right)^{1/4} 2^{7/8}K^{1-\alpha}\frac{\partial A}{\partial \zeta} = K^{\alpha/8}A\zeta^{1/2}, \quad (30)$$

and choosing $\alpha = 8/9$, we can integrate to find

$$A(r) = k\,\exp\left\{-\frac{2^{15/8}}{3^{7/4}K}(1-r)^{9/8}\right\}, \quad (31)$$

where k is a constant to be determined.

Considering the form of the solution, $A(r)t + B(r)$, we know that $A(r)$ vanishes away from the edge of the puddle, as we have already shown that there is no time dependence to the solution within the interior. Thus, $B(r)$ must match the solution at the interior at some point away from the edge. Equivalently, the total flux associated with B must match the total flux of the interior solution. Thus we can find the constant k by evaluating both sides of the following expression, a rewriting of (26):

$$-\int_0^\infty rhAK^\alpha\,d\zeta = \int_0^\infty \frac{\partial}{\partial \zeta}\left[r\left(B\frac{\partial h}{\partial r}h^3 + K\frac{\partial B}{\partial r}h\right)\right]\,d\zeta = \text{interior flux}, \quad (32)$$

or

$$-k\left(\frac{2}{3}\right)^{1/4} 2^{3/8}K^{3/9}\int_0^\infty \zeta^{3/8}(1-K^{8/9}\zeta)\exp\left\{-\frac{2^{15/8}}{3^{7/4}}\zeta^{9/8}\right\}K^{8/9}\,d\zeta = -c_s/2, \quad (33)$$

which can be re-arranged to find $k(c_s, K)$; the full expression can be found in appendix A. We compare this with the numerical solution, see figure 17, using a logarithmic axis for the concentration. The solution is fairly accurate above $r = 0.85$, improving closer to $r = 1$ as would be expected.

5.1.3 Deposition Dynamics

In order to simulate the production of speleothems, we now include deposition via a sink term in the concentration evolution equation, assuming immediate sedimentation to the bottom. We must also include an equation for the evolution of the depth of the deposit, $d(r, t)$, and therefore allow the height, $h(r, t)$ to evolve also. This results in a system of three coupled equations:

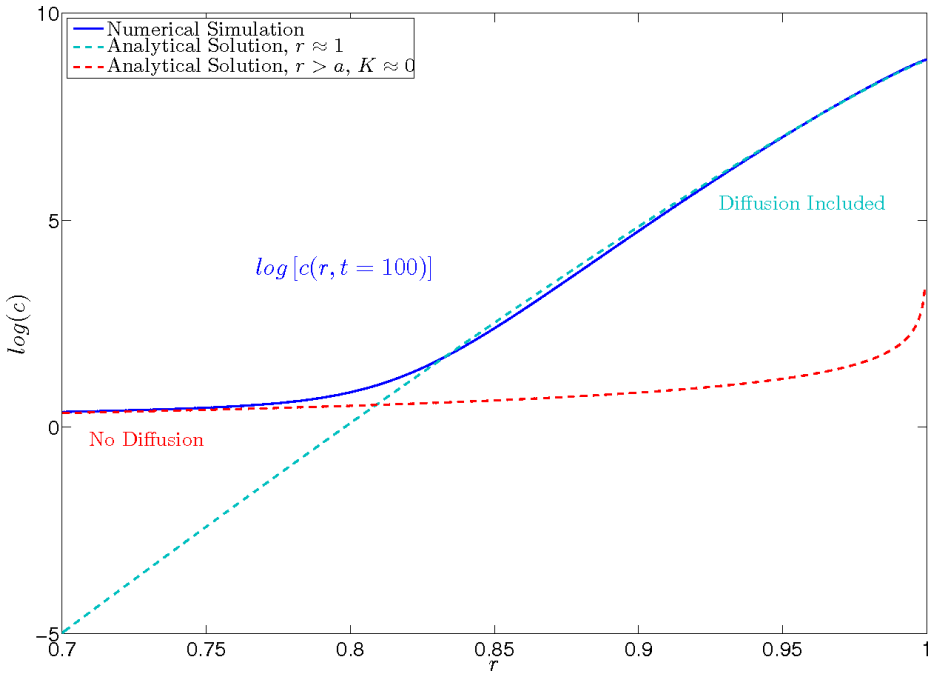

Figure 17: Comparison of the analytical solutions (31) and (24) for the concentration, c, at $t = 100$, with the numerical solution near $r = 1$. As before, $c_s = 1$, $a = 0.1$ and $K = 0.01$. The solution for $r \approx 1$ clearly improves as it approaches 1.

$$\frac{\partial (h-d)c}{\partial t} = H(a-r)\frac{c_s}{a^2} + \frac{\tau p}{H}(c_{sat} - c) + \frac{1}{r}\frac{\partial}{\partial r}\left[r\left(c\frac{\partial h}{\partial r}(h-d)^3 + K\frac{\partial c}{\partial r}(h-d)\right)\right], \tag{34}$$

$$\frac{\partial (h-d)}{\partial t} = H(a-r)\frac{1}{a^2} - \frac{L}{\sqrt{R^2 - r^2}} + \frac{1}{r}\frac{\partial}{\partial r}\left[r\frac{\partial h}{\partial r}(h-d)^3\right], \tag{35}$$

$$\frac{\partial d}{\partial t} = -\frac{\tau p}{Hs}(c_{sat} - c)(h-d), \tag{36}$$

where c_{sat} is the saturation concentration of the solute, p is a precipitation rate, s is a size scale for the concentration of crystals per depth of deposit, $R(t)$ is the boundary of the puddle and $L = \pi\kappa/q$. h and c parameters have been non-dimensionalised as before, however the time and radial parameters have been non-dimensionalized as follows: $r \to r/\lambda$, $a \to a/\lambda$, $R \to R/\lambda$, $t \to t/\sigma$, where $\lambda^2/\sigma = q/\pi H$. For limestone (Calcium Carbonate), p is a function of temperature, CO_2 pressure, and the depth of the fluid, and we take the value from [2]. The evolution equation for the depth of liquid, $(h-d)$, clearly contains a singularity at $r = R$ in the evaporation term. This unfortunately makes the system impossible to solve, as previously, using the *pdpe* routine in Matlab. Due to the limited time available on the project, it was not possible to develop an alternative method for finding a numerical solution before completion. It must also be noted that this system

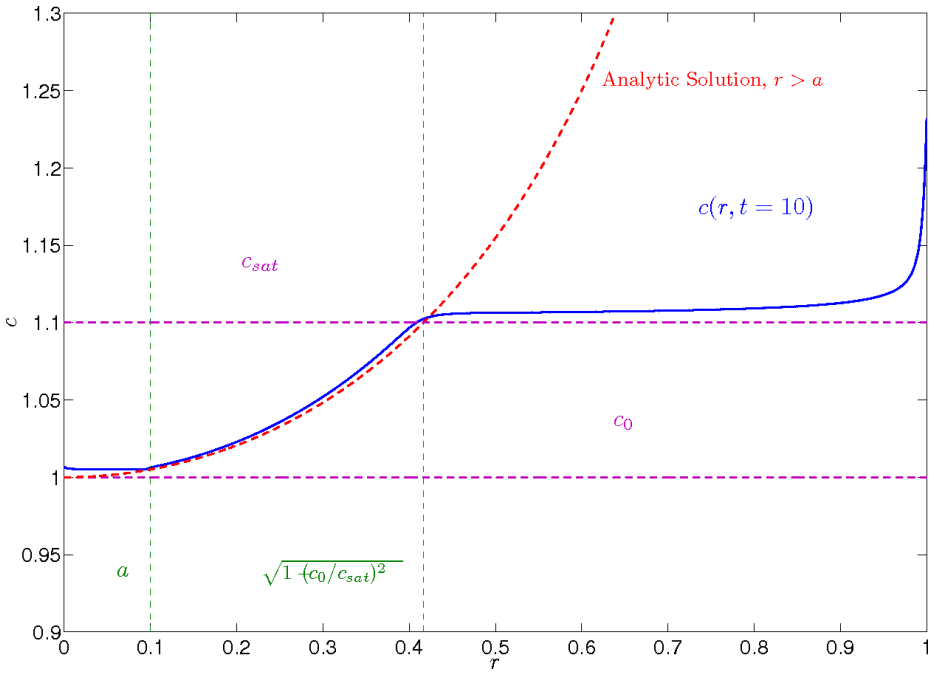

Figure 18: Numerical and analytical solutions to (34), where the solid blue line is the concentration profile $c(r)$ at $t = 10$.

now has variable boundaries, and $r = 1$ does not necessarily correspond to the edge of the puddle, and so any alternate method for solving the system would need to consider the variation in the outer boundary, $R(t)$.

We can, for small values of d, make the approximation $h >> d$, i.e. $h - d \approx h$, and so again use use the steady state form of h derived in section 5.1.1, under the assumption $\partial h/\partial t = 0$. We then calculate the depth profile, $d(r, t)$, independently from the concentration profile, $c(r, t)$. The resulting concentration profile at $t = 10$ can be seen in figure 18, where $c_s = 1$, $c_{sat} = 1.1$, $a = 0.1$, and $K = 0.01$. For $c < c_{sat}$, the same analytical solutions apply as previously, (24). For $c \geq c_{sat}$, the steady state solution is $c = c_{sat}$. It is possible to find the transition point at which $c = c_{sat}$ from (24):

$$r(c_{sat}) = \sqrt{1 - \left(\frac{c_0}{c_{sat}}\right)^2},$$

and the analytical solutions can be seen plotted in figure 18. It can be seen that the analytical solution doesn't hold near $r = 1$, where the advection and diffusion terms become important. The resulting depth profile, $d(r)$ can be seen in figure 19, along with the height profile $h(r)$, where the deposit of solute has clearly created a ring shape.

5.2 Experiments

To test the 'coffee ring' theory we first lowered the source to within a few mm of the aluminium sheet in order to first 'grow' a puddle to test the concept. Initially, the results

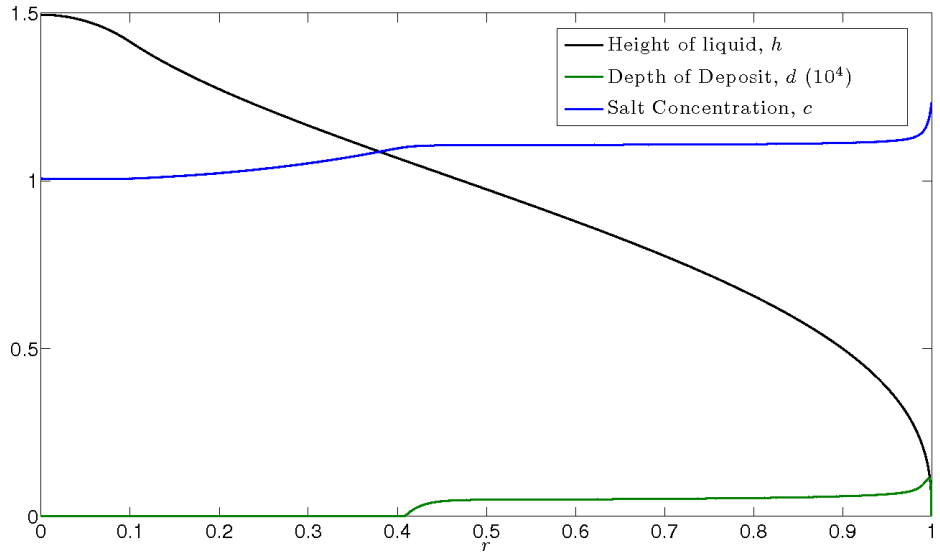

Figure 19: Solute concentration, blue, deposit depth, green, and liquid height, black, profiles at $t = 10$. Note that the deposit depth profile has been multiplied by 10^4 for clarity.

looked promising. Figure 20 shows the ring of salt produced by a puddle a few cm in diameter. However, increasing the rate of flow to grow puddles of the size required to explain the cave rings did not produce the results hoped for. Past a few cm, growth is dominated by surface tension effects at the contact line of the puddle, see figure 21. Whilst coating the aluminium sheet in vegetable oil to reduce this effect did result in a smoother boundary to the puddle, it still was not possible to produce a large, round puddle. Given that the aluminium sheet was kept as flat as was possible, and that cave floors are hardly uniform surfaces (see figure 1), this would seem to disprove the 'coffee ring' hypothesis. It was possible to find a flow rate at which evaporation matched the source flux, see figure 22, but this was definitely not a circular puddle.

The second set of experiments involved raising the source by 2m in order to see if the dynamics of the source dropping from above would affect the puddle formation. The source now arrived in drops of just under 1 ml in volume, which is similar to the volumes measured in situ by Nozzoli et al.[9]. It was found that, because the fraction of mass ejected as secondary drops was quite high, a higher flow rate was required to produce a puddle of a substantial size underneath the source. The correlation between puddle size and flow rate was expected from our model, however, while a substantial amount of crystals formed from the secondary splashes, none formed on the puddle itself, see figure 23. It is speculated that, from observations of the experiment in process, the large amount of kinetic energy imparted into the puddle by each drop effectively mixed the puddles so that the concentration profile predicted did not evolve, the solution within the puddles never exceeding saturation concentration once equilibrium was reached. As with the previous splashing experiments, see section 3.2, the salt splash formed a distribution with an exponential tail, see figure 24.

We speculated that perhaps the porosity of the cave floor might dictate the formation of the cave rings, and so repeated the experiment with piece of black cloth on top of the

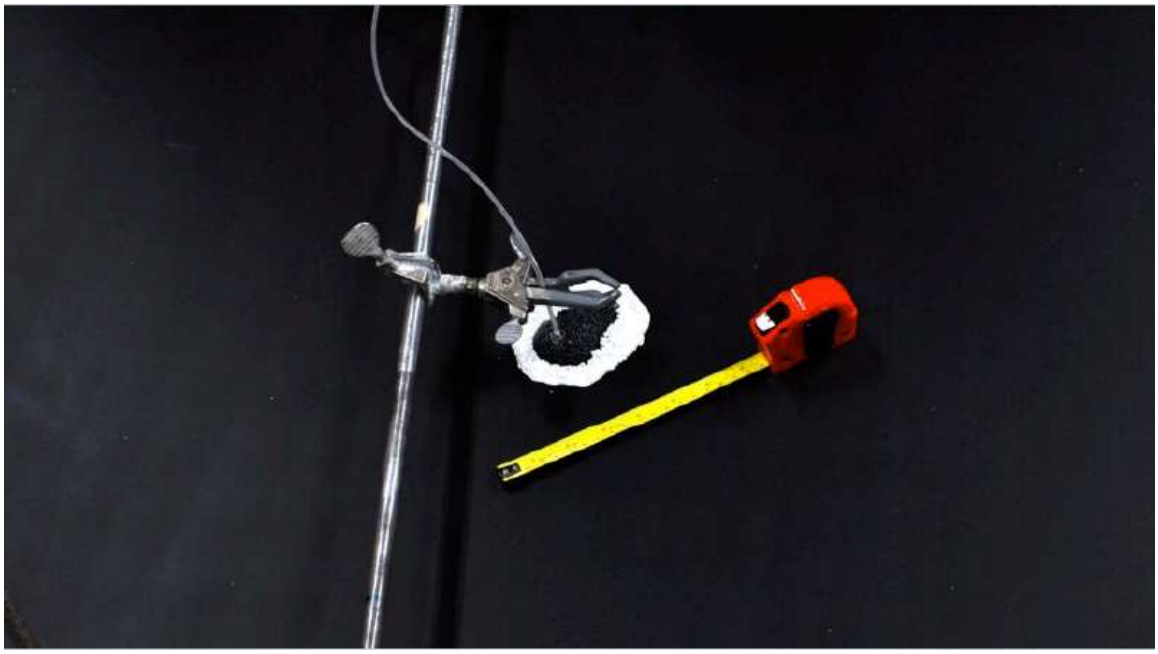

Figure 20: Initial experiment with the source close to the sheet, producing a small ring of salt. 10% salt solution was pumped at a rate of 1.4 ± 0.2 ml per hour for 46.5 hours

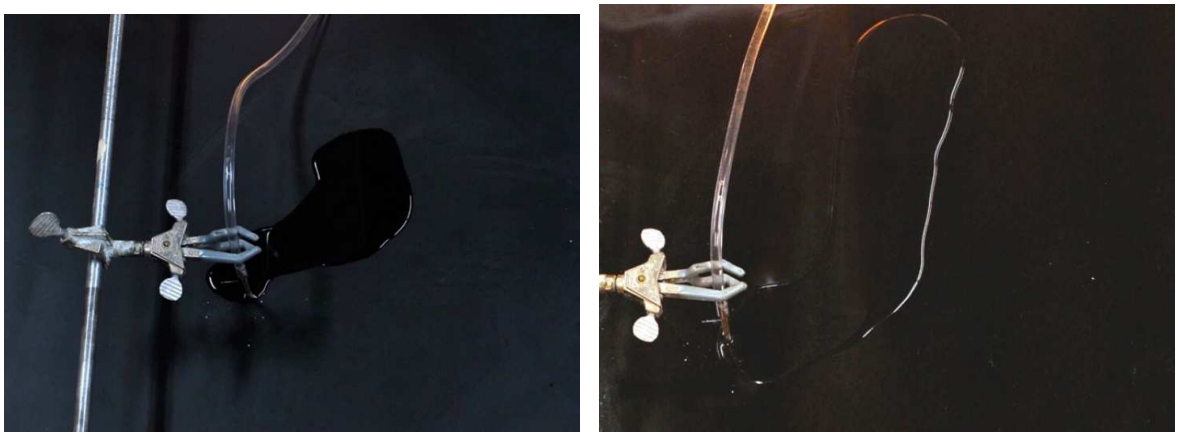

(a) (b)

Figure 21: Two experiments that show the difficulties in creating a perfectly circular puddle, both with a 10% salt solution pumped at a rate of 14.7 ± 0.7 ml per hour. (a) shows a puddle after 2.25 hrs with the original setup. (b) shows a puddle after 9 hrs, where the sheet has had a thin layer of vegetable oil applied to reduce surface tension effects.

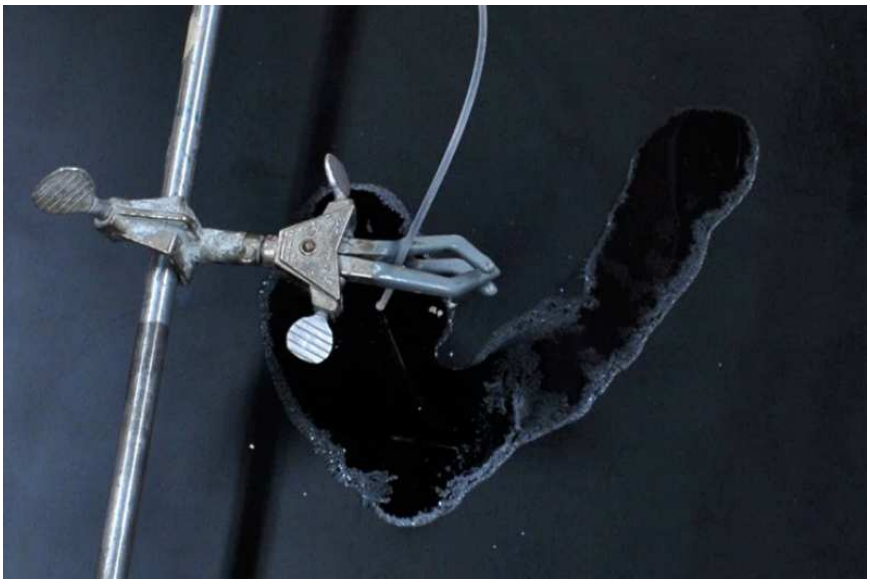

Figure 22: Experiment with flow rate of 6.4 ± 0.4 ml per hour after 5.25 hrs. Equilibrium has been reached and salt crystals are being deposited at the edge of the puddle, but the puddle is not circular.

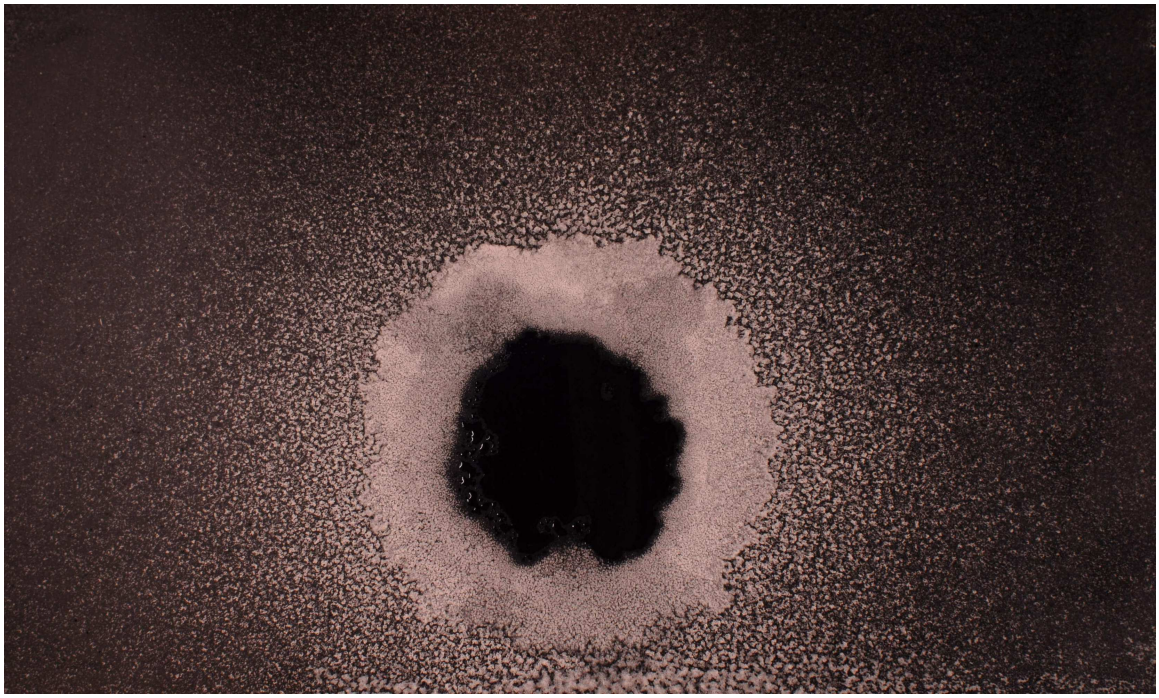

Figure 23: Experiment with source $\sim$2m above the sheet, with 10% solution being pumped at a rate of 17.17 ± 0.5 ml per hour, after 26.75 hrs. The salt deposits are produced by secondary droplets ejected from the puddle, which can be seen in the centre of the picture.

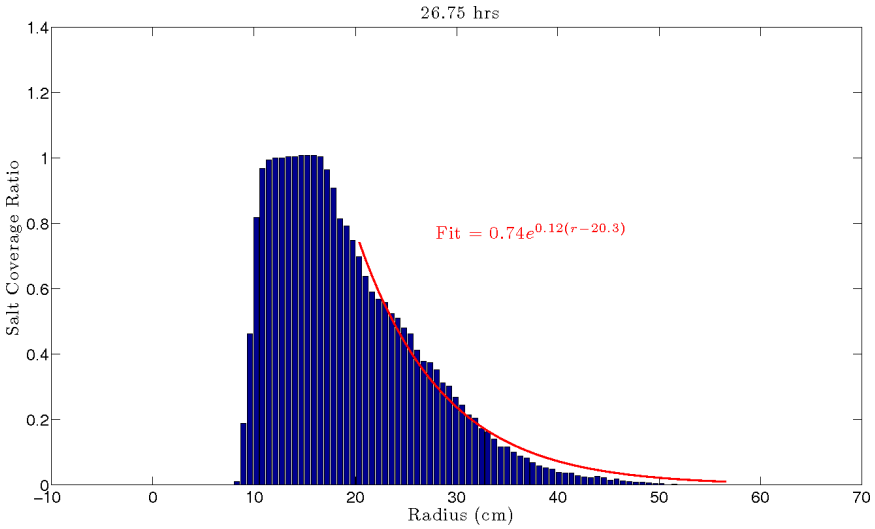

Figure 24: Salt coverage vs radius for figure 23 with an exponential curve fitted. There is a $\sim$ 10 cm ring where the area is saturated.

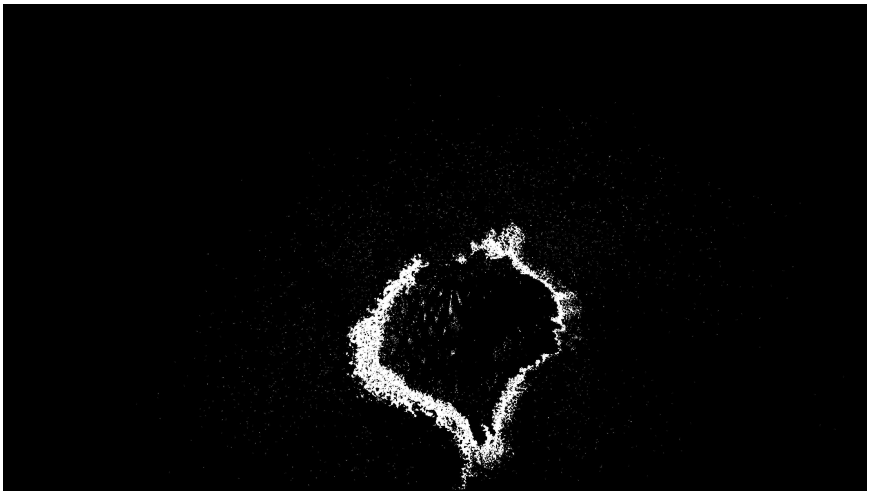

Figure 25: Experiment as previously, with black cloth covering the sheet, after 21.5 hrs. Salt has been deposited at the boundary of the wetted region, but the shape is non-uniform.

sheet, in order to test whether the spread of the puddle through a porous medium might be more uniform. The resultant salt formation can be seen in figure 25. A ring has formed, as the previous mixing of the solution within the puddle is not possible, however the shape is still non-uniform.

5.3 Speleothem Science

As it appears that the coffee ring theory is not able to describe the large cave rings observed, we turned to the science of cave formations, or speleothems. There is a huge variety of formations, but the basic method of formation is the same for most, depicted in figure 26:

- Rain water seeps down through the top layer of soil, dissolving Carbon Dioxide to form Carbonic acid.
- On contact, the acid dissolves the bedrock, normally Calcium Carbonate.
- The solution comes into contact with air on meeting a cave, and the dissolved stone is then deposited out.

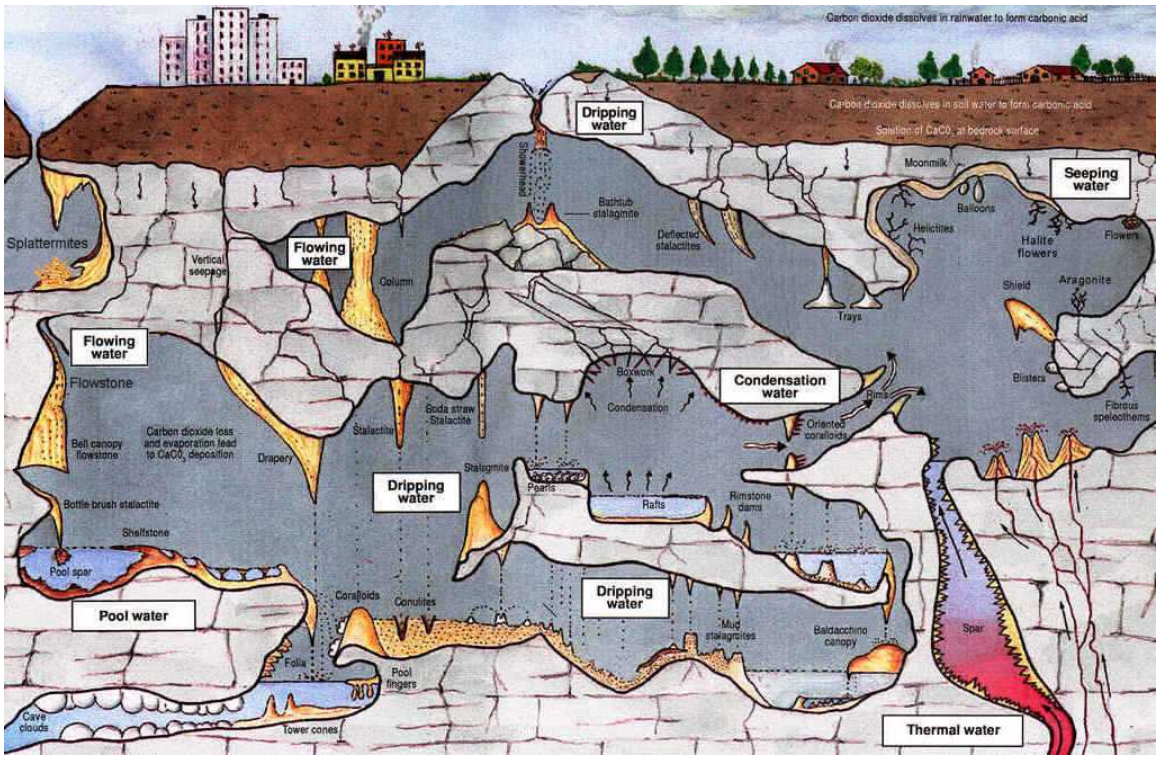

Figure 26: Depiction of the formation of speleothems, through the formation of Carbonic acid and the dissolving of Calcium Carbonate.

The overall chemical reaction involved is as follows:

$$CaCO_3 + CO_2 + H_2O \leftrightarrow Ca^{2+} + 2HCO_3^-. \tag{37}$$

The equilibrium for the reaction is towards the right, the ionic solution, when the solution is within the rock, not in contact with air. However, when the solution is in contact with the air, the chemical equilibrium moves to the left, and so CO_2 is out-gassed quickly and $CaCO_3$ deposited, as the solution is over-saturated. This is the case for the majority of formations, although in some situations, such as in highly humid regions or when the path the liquid takes is not sealed from air, the solution is under-saturated. The modelling for this project assumed that the solution was under-saturated, as is the case for the salt solution used in the experiments. As cave rings are relatively rare, it could be that they are in one of the unusual situations mentioned, however there is currently no data on the concentrations of Calcium Carbonate in the solutions forming cave rings.

It is possible to solve the model described in section 5.1.3 under the condition that the source concentration is greater than the saturation concentration, i.e. $c_s > c_{sat}$. The resulting solution at $t = 10$ for $c_{sat} = 0.5$, $c_s = 1$, is shown in figure 27. It can be seen that, although some of the solute is still swept to the edge of the puddle, most is deposited in the centre, where the source is. The resultant deposit is shaped like a classic stalagmite.

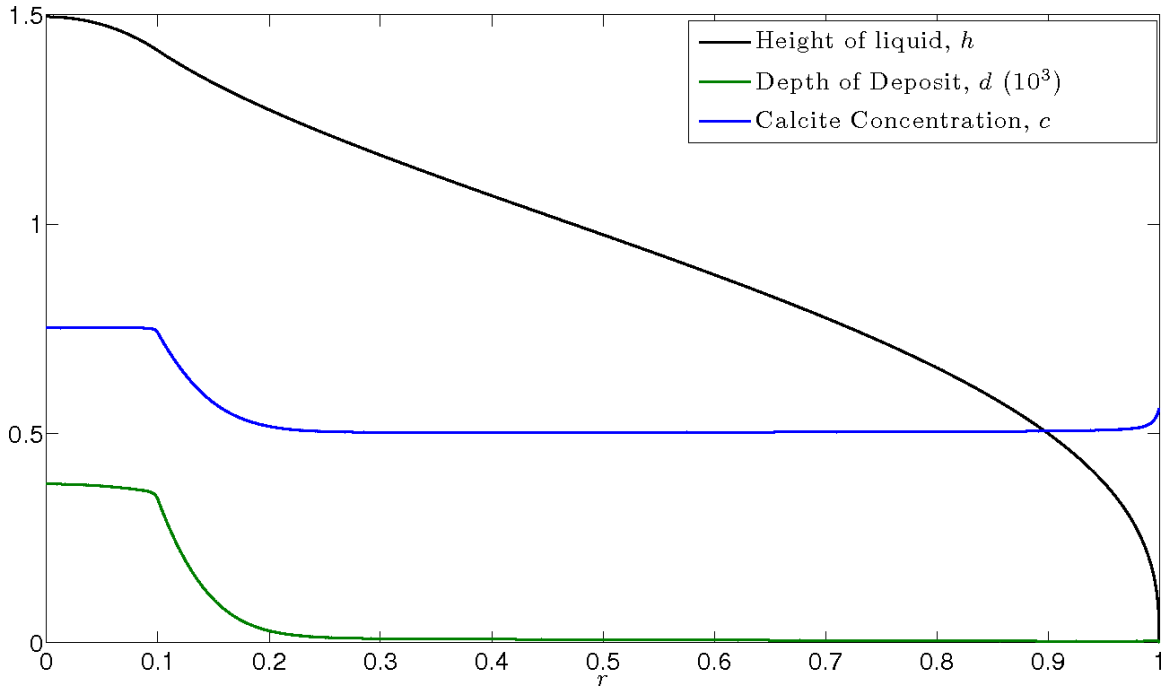

Figure 27: Numerical solution with $c_{sat} = 0.5$, $c_s = 1$, $K = 0.01$, and $a = 0.1$, at $t = 10$. The deposit depth, green line, has been scaled by 10^3 to allow for comparison.

6 Conclusion

This project set out to test the hypotheses set out in Nozzoli et al.[9] for the formation of cave rings, namely the 'splash ring' and 'fall down ring' hypotheses, and to test our 'coffee ring' theory. It was shown clearly that both the 'splash' and 'fall down' hypotheses were

unverifiable experimentally.

A mathematical model for large coffee rings was developed, and numerical solutions that matched our expectations for ring formation were produced. Unfortunately, experimentation showed that the flaw in our theory was that the formation of large, circular puddles seems to be impossible on a realistic surface, as surface tension at the contact line seems to dominate while the puddle grows, producing non-uniform shapes. Experiments also showed that the kinematics of drops arriving from 2m produces significantly different sized puddles than those where the source was close to the sheet. The majority of cave formations result from solutions that are over-saturated in Calcium Carbonate when in contact with air, whereas our experiments used under-saturated salt solution.

It seems clear that coffee rings are unlikely to be the formation method for cave rings, although there is still a little work to be done before it can be ruled out completely. Due to the limitations of the equipment and time available, it wasn't possible to create puddles larger than c. 10 cm when the source was raised 2m above the sheet. Using a higher source flux, it should be possible to see if the kinematics of the arriving drops affect the shape of larger puddles. Also, to rule out the 'fall down ring' hypothesis more comprehensively, an experiment could be designed where the source passes through a hole in a sheet, and the water collected below, in order to show that no drops split and land on the sheet.

In general, there appears to be a dearth of mathematical work in the area of speleothem formation, with an astounding range of speleothems, both beautiful and bizarre, still not understood. The development of a more accurate mathematical model for such formations could only be of benefit to the geological community.

Acknowledgements

Many thanks to both of my supervisors for the summer, Neil and Colm, who both, in their different ways, helped me stay inspired and focused throughout the project. I also wish to thank all the GFD summer fellows, who made the summer an incredibly enjoyable experience. Finally I want to thank my husband, Robert, for his continued support.

References

[1] R. F. Allen, *The mechanics of splashing*, Journal of Colloid and Interface Science, 124 (1988), pp. 309–316.

[2] D. Buhmann and W. Dreybrodt, *The kinetics of calcite dissolution and precipitation in geologically relevant situations of karst areas. 1. open system*, Chemical Geology, 48 (1985), pp. 189–211.

[3] R. D. Deegan, O. Bakajin, T. F. Dupont, G. Huber, S. R. Nagel, and T. A. Witten, *Contact line deposits in an evaporating drop*, Physical Review E, 62 (2000), pp. 756–765.

[4] G. German and V. Bertola, *Formation of viscoplastic drops by capillary breakup*, Physics of Fluids, 22 (2010).

[5] C. Hill and P. Forti, *Cave minerals of the world*, National Speleological Society, 2nd ed., 1998, pp. 94–95.

[6] H. Hu and R. G. Larson, *Evaporation of a sessile droplet on a substrate*, The Journal of Physical Chemistry B, 106 (2002), pp. 1334–1344.

[7] N. N. Lebedev, *Special functions and their application*, Prentice-Hall, 1965.

[8] L. Montanaro, *Osservazioni sui "cherchi" della Grotta del Sorell*, Bollettino del Gruppo Speleologico Sassarese, 13 (1991-1992), pp. 21–22.

[9] F. Nozzoli, S. Bevilacqua, and L. Cavallari, *The Genesis of Cave Rings explained using Empirical and Experimental Data*, Journal of Cave Karst Studies, 71 (2009), pp. 130–135.

[10] A. I. J. M. Van Dijk, A. G. C. A. Meesters, and L. A. Bruijnzeel, *Exponential distribution theory and the interpretation of splash detachment and transport experiments*, Soil Science Society of America Journal, 66 (2002), pp. 1466–1474.

[11] E. Villermaux and B. Bossa, *Single-drop fragmentation determines size distribution of raindrops*, Nature Physics, 5 (2009), pp. 697–702.

A Full Concentration Solution

In section 5.1.2, the time dependent part of the solution to (21) close to the edge of the puddle at large t, A, is set out in (31), where the constant, k, is given by (33). Rearranging, we find

$$\begin{aligned} k(c_{sat}, K) &= \frac{3^{1/4}}{2^{13/8}} c_{sat} \Bigg[K^{11/9} \int_0^\infty \zeta^{3/8} \exp\left\{ -\frac{2^{15/8}}{3^{7/4}} \zeta^{9/8} \right\} d\zeta \\ &\quad - K^{19/9} \int_0^\infty \zeta^{11/8} \exp\left\{ -\frac{2^{15/8}}{3^{7/4}} \zeta^{9/8} \right\} d\zeta \Bigg]^{-1}, \qquad (38) \\ &\approx \frac{3^{1/4}}{2^{13/8}} c_{sat} \left[1.74 K^{11/9} - 3.48 K^{19/9} \right]^{-1}, \qquad (39) \end{aligned}$$